Geomorphology 336 (2019) 152–164

Contents lists available at ScienceDirect

Geomorphology

journal homepage: www.elsevier.com/locate/geomorph

Assessing patterns of annual change to permafrost bluffs along the North Slope coast of Alaska using high-resolution imagery and elevation models

Ann E. Gibbs [a,*], Matt Nolan [b], Bruce M. Richmond [a], Alexander G. Snyder [a], Li H. Erikson [a]

[a] U.S. Geological Survey, Pacific Coastal and Marine Science Center, 2885 Mission Street, Santa Cruz, CA 95060, USA
[b] Fairbanks Fodar, P.O. Box 82416, Fairbanks, AK 99708, USA

ARTICLE INFO

Article history:
Received 5 October 2018
Received in revised form 20 March 2019
Accepted 25 March 2019
Available online 29 March 2019

Keywords:
Coastal change
Permafrost bluffs
Arctic Alaska
Beaufort Sea

ABSTRACT

Coastal permafrost bluffs at Barter Island, on the North Slope, Beaufort Sea Coast of Alaska are among the most rapidly eroding along Alaska's coast, having retreated up to 132 m between 1955 and 2015. Here we quantify rates and patterns of change over a single year using very-high resolution orthophotomosaics and co-registered surface elevation models derived from a survey-grade form of structure-from-motion photogrammetry from a fixed-wing, manned aircraft. The resulting elevation models were validated with over 10,000 ground check points and found that 95% agreed to within 20 cm, before accounting for real differences in the ground surface due to seasonality, vegetation, and checkpoint acquisition errors. This data set provides the most detailed and accurate measurements of coastal change to date along the Alaskan coast and the method is scalable to more extensive coastlines. Between July 2014 and July 2015, the bluffs retreated an average of 1.3 m, and a maximum of 8.1 m, with an associated net volume loss of 38,100 ± 300 m^3 (1.3 m^3/m). This average retreat over this single year was slightly less than the 60-year mean rate of change of −1.5 ± 0.1 m/yr, suggesting the 2014–2015 year represented relatively typical to slightly below average conditions. Most of the bluff material (70%) was lost during the 3 summer months (July to Sept) of 2014 and the remaining 30% between the late-summer and following winter-spring. The pattern of change was predominantly landward retreat of the top of the bluffs, removal of the debris apron and subsequent niching at the base of the bluffs during mid to late summer (July to Sept) followed by erosion of the bluff face and deposition of debris at the base of the bluff through the remainder of the year (Sept to the following July). Drivers of the observed change are likely a combination of thermal erosion on the bluff face throughout the summer and episodic thermo-mechanical removal of material, niching, and undercutting of the base associated with high-water levels driven by low-pressure storms and westerly winds. These patterns and high rates of change are believed to be broadly representative of coastal permafrost bluffs found along many high-latitude coastlines worldwide.

1. Introduction

Arctic permafrost coasts represent about 1/3 of the world's coastlines (Lantuit et al., 2012) and are unique from temperate coasts in that their behavior is strongly influenced by the presence of interstitial ice and permafrost, which provide cohesion to relatively unconsolidated material, and the presence, absence, and duration of seasonal sea-ice (Aré, 1988; Reimnitz et al., 1988). Processes driving coastal change in permafrost environments can be fundamentally reduced to mechanical and thermal processes and shorelines anchored by permafrost-rich substrates are highly vulnerable to climate change, as increasing temperatures and duration of the ice-free season and degradation of permafrost can lead to accelerated rates of coastal erosion (Overeem et al., 2011; Barnhart et al., 2014; Jones et al., 2018). Despite this vulnerability, our understanding of how these coastal environments change through time is poor due to the remoteness of these locations, limited windows of opportunity for observation (limited daylight and ice-free conditions), poor geodetic infrastructure, scarcity of historical data, and other data collection challenges. Recent advances in coastal change and, in particular, permafrost bluff change research in the Arctic, for example in Western Siberia (Isaev et al., 2018; Novikova et al., 2018), Svalbard (Guégan and Christiansen, 2017), and the Canadian Arctic (Obu et al., 2017; Irrgang et al., 2018) have improved the overall scientific understanding of the diverse forms and rates of coastal change across the Arctic, however, high quality, highly accurate, and

* Corresponding author.
E-mail addresses: agibbs@usgs.gov (A.E. Gibbs), matt@fairbanksfodar.com (M. Nolan), brichmond@usgs.gov (B.M. Richmond), agsnyder@usgs.gov (A.G. Snyder), lerikson@usgs.gov (L.H. Erikson).

https://doi.org/10.1016/j.geomorph.2019.03.029

temporally robust field data from which to confidently assess and/or impacts of climate change are still lacking (Lantuit et al., 2013; Overduin et al., 2014). Extreme erosion of the Alaskan Beaufort Sea coast has been observed for well over a century, with estimates of highly variable erosion rates on the order of 1 to 10 m per year (m/yr), witnessed by Ernest Leffingwell during his 1906–1914 expeditions (Leffingwell, 1919). More recently, using topographic maps, orthoimagery, and lidar data, Gibbs and Richmond (2015, 2017), calculated an average long-term shoreline change rate of −1.8 ± 0.04 m/yr along the Alaskan Beaufort Sea coast between 1947 and 2012, and with much higher rates (up to 22 m/yr of retreat and 11 m/yr of deposition) measured at some locations. Lantuit et al., 2012 summarized coastal change rates for the approximately 25% of the Arctic coast where coastal change rates were measured and found that arctic coastlines are eroding at an average rate of 0.5 m/yr, but with considerable local and regional variability. The highest mean rates of erosion were measured in the Laptev (0.73 m/yr), East Siberian (0.87 m/yr), and Canadian and American Beaufort Seas (1.12 and 1.15 m/yr, respectively). These long-term rates are more than three times higher than for most other predominantly erosional, temperate coasts of the U.S. (Hawaii, Fletcher et al., 2012; New England and Mid-Atlantic, Hapke et al., 2011; and the Gulf and Southeast, Himmelstoss et al., 2017). Only along the Gulf Coast of Louisiana are mean erosional long-term shoreline change rates higher (−7.7 ± 0.9 m/yr from 1853 to 2001), primarily due to the migration of barrier islands and permanent loss of wetlands thought to be associated with submergence and destruction of the Mississippi River delta plain (Reimnitz et al., 1988; Penland et al., 1990; Morton et al., 2004; Himmelstoss et al., 2017). When comparing annually averaged rates, however, it's important to recognize that in contrast to temperate environments where coastal processes can modify the coast for 12 months of the year, most of the coastal change in high-latitude permafrost environments occurs only during the ~3-month long, ice-free season when winds, waves, and coastal currents can act directly on an exposed coast (Wiseman Jr. et al., 1973; Hopkins and Hartz, 1978). As the duration of ice-free conditions increases, the potential for greater coastal change increases, especially as coastal sea-ice forms later in the year, leaving the coast vulnerable to the impacts of large fall storms.

Long-term, multi-year rate change analyses provide important information on overall trends and patterns and can be compared with rates of change from other locations, however, details on timing and processes and an understanding the interplay between the two in the overall pattern of change requires detailed observation and measurements acquired at appropriate time scales. For example, is erosion gradual or episodic, and under what circumstances? Or, are erosion rates accelerating and what are the significant processes driving the change? The ability to quantify coastal change and understand these patterns and drivers at appropriate time scales is important for modeling and projecting future coastal behavior, especially as arctic air and water temperatures increase and stronger and more frequent storms can impact the coast later in the season as seasonal sea-ice forms later and melts earlier (Barnhart et al., 2014). Along the extensive and remote coast of Alaska, high-quality imagery and elevation data are historically rare, in part because traditional methods of acquiring the data are cost prohibitive. Recent advances in digital photogrammetric technology, including improvements to consumer-grade cameras, GPS processing techniques, desktop computer processing capabilities, and the development of powerful photogrammetric software using Structure-from-Motion (SfM) algorithms (Koenderink and van Doorn, 1991; Westoby et al., 2012; Nolan et al., 2015; Nolan and DesLauriers, 2016), allow for improved mapping and analysis of coastal change in 3-dimensions for a fraction of the cost of traditional photogrammetric or lidar technologies.

The goal of this paper is to document and quantify an annual pattern of 2- and 3-dimensional change to the coastal permafrost bluffs at Barter Island, Alaska using repeat, airborne orthoimagery and coincident digital surface elevation models (DSMs) derived using SfM photogrammetric methods and precise positioning. The technique is not only well suited to rapidly acquiring high quality data in remote locations, but can also be applied in most environments for a fraction of the cost of lidar or traditional photogrammetric acquisition and where ground- or unmanned aircraft system (UAS)-based surveys are impractical. Using time-lapse cameras and water level and temperature measurements we infer the timing of observed change and discuss implications in the context of sediment budget, annual signals, and relative mechanisms of change. Despite the limited time span of this study, the results shed light on the rapid rates of coastal change along high-latitude shorelines where changing climate conditions have the potential to alter the behavior of these coastal environments, particularly through accelerated thermal degradation and increased mechanical erosion during extended periods of ice-free, open-water conditions.

2. Study location

Barter Island, considered the gateway to the Arctic National Wildlife Reserve (ANWR), is located on the northeast coast of Alaska approximately 120 km west of the U.S.-Canadian border on the Alaskan Beaufort Sea coast (Fig. 1). The island has a long history of Inupiat occupation and was a major trade center until the late 19th century (State of Alaska, 2015). The Native Village of Kaktovik on the north shore of Barter Island was incorporated as a city in 1971 and had a population of 239 as of the 2010 census. Like other Native Villages in northern Alaska, subsistence hunting, fishing and whaling play a major role in the local economy and lifestyle. In the 1950s, the U.S. Air Force built an airstrip and Defense Early Warning Line (DEW) radar station on the island. The DEW site was deactivated in 1989 and in 1990 upgraded to part of the North Warning System Long Range Radar Site (LRRS) which continues operations today. Access to the island is limited to boats, barges, and aircraft – there are no permanent roads leading to the island (Fig. 1).

The village of Kaktovik and adjacent U.S. Air Force radar site are fronted by eroding coastal permafrost bluffs that range in height from a few meters to more than ten meters high. Barter Island, like the entire North Slope of Alaska, is in a zone of continuous permafrost, with a shallow active layer (generally <1 m deep) that is subject to thawing during the summer season. The coastal permafrost bluffs are poorly consolidated and consist of a complex sequence of material ranging from dense clay, interbedded sand and gravel, massive sand, widespread ground ice including ice wedges, segregated ice layers, massive ice, and thermokarst cave ice, and a surface peat layer (Rawlinson, 1993; Jorgenson and Brown, 2005; Kanevskiy et al., 2013). Aerial lidar elevation data obtained in 2009 (U.S. Geological Survey, 2015) revealed ~10 m high bluff elevations across the central portion of the island where field observations of bluff stratigraphy showed multi-layered

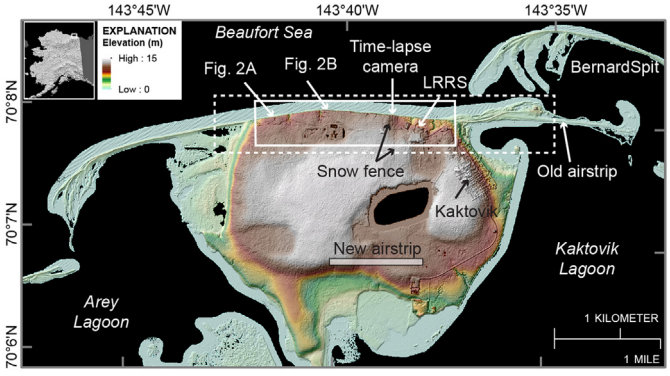

Fig. 1. Lidar derived elevation map of Barter Island showing locations described in the text. Solid white box outlines the bluff study area and location of Fig. 5. Dashed white box outlines the boundary of Fig. 3.

stratification. The lower elevation outer flanks of the exposed bluff face consist of layers of sandy-silt below the surface peat layer. The island has broad, low-lying (< 2 m high) sand and gravel barrier spits extending both east and west from the topographically higher tundra hinterland of the island.

The Beaufort Sea is typically covered with sea ice from approximately October through June. Prevailing winds are easterly and average near 21 km/h (13 miles/h) with little annual variation (Western Regional Climate Center, 2008; Zhang et al., 2016). The region is microtidal with a mean diurnal range of 18 cm (0.6 ft.; NOAA, 2017a), however, water levels can become elevated or depressed up to several meters due to winds and low-pressure systems; westerly winds tend to elevate water levels, whereas easterly winds tend to lower water levels (Reimnitz and Maurer, 1979; Sultan et al., 2011; Erikson et al., in press).

Using topographic maps, orthoimagery, and lidar elevation data from 4 times periods between 1947 and 2012, Gibbs and Richmond, 2017 found average rates of change of the shoreline fronting the Barter Island coast of −1.2 ± 0.2 m/yr (range −1.8 to +0.2 m/yr) and bluff retreat rates averaged 1.5 ± 0.1 m/yr (range 2.2 to 0.4 m/yr) between 1955 and 2015 (Gibbs et al., 2018). The long-term rates can be punctuated by individual years with much higher erosion rates and over 20 m of bluff retreat has been observed by the authors in a single year (e.g. 2008, 2017). Mechanisms for bluff failure along this coast are poorly documented but likely include a combination of thermal degradation and thawing of permafrost in the exposed bluff face (thermodenudation), mechanical and thermal niching at the bluff toe, followed by rotational slumping and block collapse (thermoabrasion; Aré, 1988; Hoque and Pollard, 2009; Günther et al., 2013). Recession rates appear to be largely dependent on ice content, the frequency and intensity of storms, run-up elevation, and seawater and air temperatures (Reimnitz et al., 1988; Wobus et al., 2011; Overduin et al., 2014).

3. Methods

3.1. Image acquisition and construction of elevation models

A proprietary form of structure-from-motion photogrammetry known as fodar was used to acquire and create orthophotomosaics and digital elevation models. Image acquisition methods and hardware are described fully in Nolan et al. (2015), Nolan and DesLauriers (2016), and Gibbs et al. (2016) and did not deviate significantly for this study. A key feature of fodar is that photo-center positions are located to within 10 cm using on-board survey-grade GPS and proprietary hardware. Acquisitions were made on 3 separate dates and flight lines, altitudes, and resolution of the data were different for each of the surveys (Table 1). The July 2014 survey was opportunistic and reconnaissance in design and not optimized for resolution and precision compared to the later surveys. Orthophotomosaics, digital surface models, raw and edited elevation point clouds, and supporting GPS data used in this study are available at Gibbs et al., 2019).

[GCP, Ground Control Point].

Prior to DSM generation the elevation point cloud was edited to remove structures and spurious elevation values associated with moving water surfaces. DSMs were created using a uniform 23-cm cell size, natural neighbor algorithm, and half-meter point thinning method in ArcMap (ESRI, 2014) and areas where snow and ice were present in the imagery, particularly July 2014, were masked from the final DSMs prior to volume change analyses. Permafrost bluffs along the Arctic coast commonly have a surficial peat layer that is more cohesive and resistant to erosion than underlying, less consolidated but ice rich sands and gravels. As bluffs erode this can result in overhanging visor morphology at the top of the bluff and a more landward (southerly) position of the underlying face and/or base of the bluff (Fig. 2A). In this study, bluffs were photographed from a position slightly seaward of the beach and nearly the entire face of the bluff was imaged and real elevations calculated for both the upper sub-horizontal visored tundra surface as well as the bluff face. In some locations, this resulted in a wide range of Z (elevation) values for the same or adjacent X and Y locations (Fig. 2B) and a simple averaging of all the elevation points in locations with a large *Z*-value range would yield lower net values than the true value of the top of the bluff. To resolve this, a conditional raster representing the range of elevation values contained within one square meter was created and, using this conditional raster, the maximum value within the specified grid cell size (upper surface) was selected where the range of elevation values exceeded 1 m. Where range of elevation values were <1, a simple average of the points within the grid cell was calculated.

3.2. Ground control and check points

Ground survey data were acquired in September 2014 and 2016 using dual frequency GPS receivers and post-processed relative to a

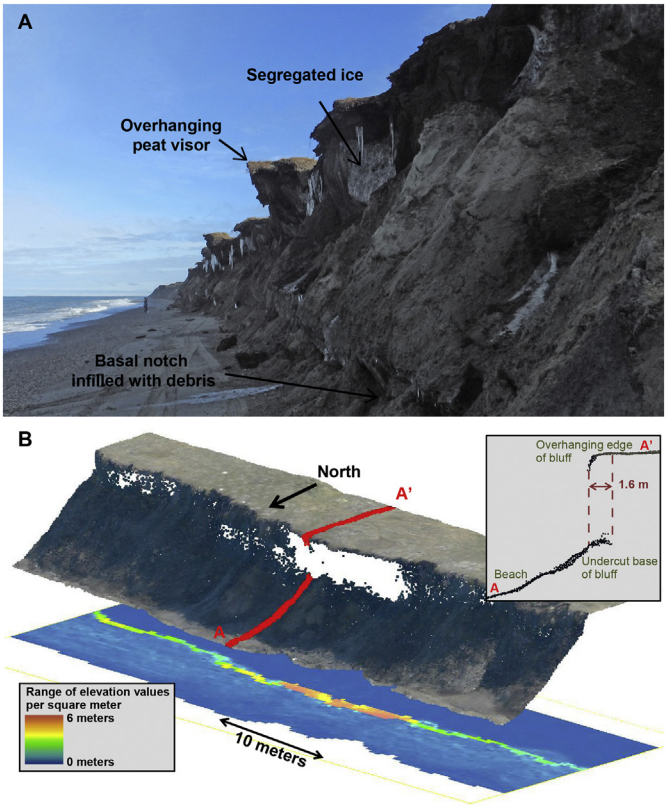

Fig. 2. A: Photograph of the bluffs at Barter Island showing overhanging peat visors at the top of the bluffs underlain by a thick layer of segregated ice and unconsolidated sand and gravel that are notched at their base and partially infilled with debris; bluff height is approximately 8 m (Photo A. Gibbs, Sept. 2016); B: Example of the point cloud data from July 2015 for a small section of the Barter Island Coast. The colored band shows the range in elevation values within 1 square meter. Profile A-A' across the point cloud data shows that where the edge of the bluff top is overhanging, elevation data from both the top and upper face of the bluff have significantly different Z values for shared X and Y locations. Elevation data is missing where bluffs features were not resolvable by the SfM process.

Table 1
Data acquisition and adjustment parameters.

Date	Altitude (m)	Resolution (cm)			Adjustment to GCP (cm)		
		Image	$RMSE_r$	DSM	X	Y	Z
Jul 01, 2014	740	19	19	23	−7	17	132
Sep 07, 2014	450	11	11	23	−13	−19	36
Jul 05, 2015	320	8	8	23	−6	−12	32

temporary base station on Barter Island. Data were collected at 3 photo-identifiable survey monuments in 2014 and 2016, along 9 transects across the tundra bluff in September 2014, and in September 2016 at additional points located on the concrete and gravel pads near the former POL (Petroleum, Oil, and Lubricants) tank farm north of the LRRS that are presumed to have remained vertically stable over the past few years (Fig. 3). Horizontal and vertical accuracy of the data are approximately ±0.03 m. Vertical elevations of the bluff transect data that were acquired by walking with the survey rod held slightly above the ground surface could be biased upward by 5 to 10 cm.

Data were shifted to best fit the coordinates of the survey monument closest to the bluff change study area, CP-3, as measured in September 2016. (Horizontal datum: WGS84 UTM Zone 7; Vertical datum WGS84 ellipsoid; Table 1). To validate accuracy, the shifted datasets were then compared to the survey monuments, bluff transects, and additional photo-identifiable features and residual offsets, RMSE, and standard deviation between the data sets were calculated (Tables 1 and 2).

3.3. Feature extraction and change analysis

Two and 3-dimesional change analyses were completed for the 3.2 km stretch of the bluffed coast (Fig. 1). Two-dimensional features, including the position of the bluff edge (top and base) and the shoreline, were delineated using a combination of the orthoimagery, elevation, and hillshade and slope rasters. The bluff top edge was digitized visually and is estimated to be within ±1 m. The base of the bluff and shoreline are defined as the −0.5 m and −1.6 m contours (WGS84 ellipsoid), respectively. In some locations, particularly on the east and west ends of the study area, the −0.5 m contour included some beach material but it generally coincided with the seaward edge of the bluff or debris apron. Where more than one −1.5 m contour was present on the beach (for example, where there was a swale or cat-eye pond) the seaward most contour was chosen to represent the shoreline. Change in the position of the 3 features was calculated every 10 m alongshore using the Digital Shoreline Analysis System (Thieler et al., 2009).

Net sediment volume change of the coastal bluffs was calculated by differencing the DSMs for the 3 time periods. The surfaces were subtracted from one another and, in order to restrict the change analysis to the active bluff area, and not the adjacent beach, the difference surfaces were clipped to an active bluff polygon area defined by the top of bluff and the −0.5 m contour for each respective time period. The results were multiplied by the raster pixel area (0.23 × 0.23 cm) to produce the net volume change in cubic meters. These net volume change values were normalized using the individual active bluff polygon areas for each analysis period to provide a relative value of volume change in cubic meters per meter (Table 3).

3.4. Accuracy and error analysis

In contrast to more developed coastlines, little fixed infrastructure or geodetic control points exist on the rural and relatively undeveloped northern Alaska coast. Dirt and gravel roads and airstrips are continually graded and regional and local changes in ground elevations associated with permafrost thawing (subsidence) and freezing (heave) are not

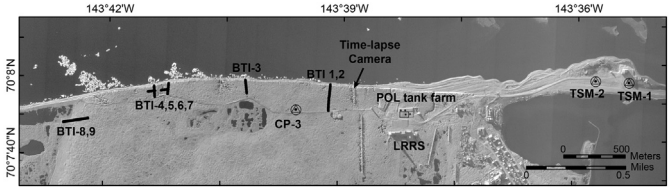

Fig. 3. Location map showing the time-lapse camera, ground control points (CP-3, TSM-1, TSM-2), cross-tundra transects (BTI1–9), and the former POL tank farm pad over which the vertical uncertainty was calculated.

Table 2
Summary statistics for DSM versus GPS elevations for surveyed locations.

Image Date	n	RMSEz	Max offset (m)	Mean offset (m)	StDev
Photo-identifiable survey monuments					
Jul-14	7	0.11	−0.21	−0.08	0.09
Sep-14	7	0.09	0.15	0.07	0.06
Jul-15	7	0.11	−0.13	0.04	0.11
Stable ground features					
Jul-14	1182	0.04	−0.12	−0.02	0.03
Sep-14	1182	0.03	0.08	−0.02	0.02
Jul-15	1182	0.03	−0.08	−0.02	0.02
9 cross-bluff transects					
Jul-14	9818	0.09	0.27	0.00	0.09
Sep-14	9818	0.13	0.35	−0.08	0.10
Jul-15	9818	0.21	0.12	−0.19	0.09
All points					
Jul-14	11,007	0.08	0.27	0.00	0.08
Sep-14	11,007	0.12	0.35	−0.07	0.10
Jul-15	11,007	0.20	0.15	−0.17	0.10

well constrained or understood but can be on the order of decimeters (Shiklomanov et al., 2013; Liu and Larson, 2018).

Extensive testing of the accuracy, precision and noise level of fodar photogrammetry used here is discussed in Nolan et al. (2015) as part of a study mapping snow depths from manned aircraft. In that study, geolocation accuracy of the DSMs was found to be within ±30 cm at 95% confidence without use of ground control, with the vertical misfit typically being the largest. The precision (repeatability) was about ± 8 cm at 95% confidence. In the coastal study presented here, we found less than ±20 cm horizontal difference between the surveyed ground control monument (CP-3) and the unshifted orthoimagery for all data sets (Table 1). Vertical differences were similar in September 2014 and July 2015 (36 cm and 32 cm lower than the surveyed ground control, respectively) and 132 cm below surveyed ground control for July 2014 (Table 1). This larger difference in July 2014 may be due to less stringent image acquisition and positioning parameters, as this data set was reconnaissance in design. Once shifted, horizontal residuals were equal to the resolution of the image data set and vertical residuals over stable areas were within a few centimeters (Tables 1 and 2).

Comparison of shifted imagery and DSMs to other ground features in order to assess any large scale spatially-coherent noise (such as warps, tilts, rolls etc.) or bias in the DSM was done by comparing DSM and GPS elevations at the GCPs and along the 9 cross-bluff transects. A nearly 1:1 correlation was found between the two with some variability, but overall maximum offsets were <35 cm, mean offsets <19 cm, and RMSE values <21 cm (Table 2). The difference between surveyed ground control point elevations, which include only fixed monuments and points assumed to be vertically stable, and DSM elevations show the smallest and most consistent residual of 6 cm. Residuals along the 9 cross bluff transects show the most variability, partly due to the fact that DSM elevations are not true 'bare earth' and can represent points on the ground or tops of vegetation, although tundra vegetation is sparse and generally less than about 30 cm high. GPS survey elevations measured along the bluff transects may also be biased upward by up to 10 cm due to measurement techniques. Real differences in ground elevation between surveys might also be expected due to seasonal changes in vegetation height or variations in relative vertical ground elevation in response to seasonal thaw subsidence.

To evaluate uncertainty in volumetric change we derived an empirical uncertainty based on measured volume changes over an unvegetated and assumed stable area where no change would be expected between survey periods. For this analysis we chose the circular concrete pads at the former POL tank farm north of the LRRS (3204 m^2, Fig. 3), as these large features are likely the most stable vertical targets on the island, with the added advantage of serving as useful

Table 3
Bluff change results and uncertainty values.

Time period	Active bluff area (m^2)	Vertical change (m)			Volume change				
		Min	Max	Mean	Net (m^3)	Uncy (m^3)	Net (m^3/m)	AUncy (m/m)	% of area
Study area									
Jul14 to Sep14	28,429	−8.57	1.18	−0.94	−26,700	±700	−0.94	±0.02	100
Sep14 to Jul15	24,487	−6.10	2.06	−0.50	−12,300	±300	−0.50	±0.01	100
Jul14 to Jul15	29,602	−8.30	0.85	−1.29	−38,100	±300	−1.29	±0.01	100
West bluffs									
Jul14 to Sep14	7689	−4.01	0.57	−0.63	−4900	±200	−0.63	±0.02	27
Sep14 to Jul15	7379	−3.25	2.06	−0.18	−1300	±100	−0.13	±0.01	26
Jul14 to Jul15	8172	−3.66	0.64	−0.70	−5700	±100	−0.70	±0.01	29
Central bluffs									
Jul14 to Sep14	16,630	−8.57	0.48	−1.33	−22,100	±400	−1.33	±0.02	68
Sep14 to Jul15	12,860	−6.10	1.26	−0.91	−11,700	±100	−0.91	±0.01	53
Jul14 to Jul15	17,307	−8.30	0.67	−1.92	−33,300	±200	−1.92	±0.01	71
East bluffs									
Jul14 to Sep14	4110	−1.13	1.18	0.06	300	±90	0.06	±0.02	14
Sep14 to Jul15	4248	−0.71	0.78	0.16	700	±50	0.16	±0.01	14
Jul14 to Jul15	4123	−0.86	0.85	0.22	900	±50	0.22	±0.01	14

[Min, minimum; Max, maximum; Uncy, uncertainty; AUncy, area-averaged uncertainty].

horizontal alignment tools and not being affected by seasonal vegetation growth. Within this area we calculated an area-averaged vertical difference of −0.02 m, −0.01 m, and − 0.03 m for the analysis periods Sept 2014-July 2014, July 2015-Sept 2015, and July 2015–July 2014, respectively. The total active bluff area was multiplied by these area-averaged differences to determine a total uncertainty in m^3 on our volume change calculations (Table 3). Additional sources of uncertainty, such as seasonal differences in tundra vegetation height or thaw subsidence, are considered to be small and/or random and were not included in the error analysis.

Overall the resolution and accuracy of this dataset is superior to currently available airborne-derived datasets along the Beaufort Sea coast, with image resolutions <20 cm and DSM resolutions of 23 cm with a vertical RMSE of 3–4 cm on stable survey points and <20 cm RMSE on over 11,000 points measured across a variety of land surfaces.

3.5. Time-lapse imagery

A time-lapse game camera deployed during the summer of 2014 at the bluff edge near the snow fence west of the LRRS collected still photographs and video to document bluff, beach, and wave conditions throughout the summer. The camera recorded at a fixed rate of 1 still frame per hour and video triggered by movement in the field of view. Examples of images acquired show a transition from late spring (June 15, 2014), when the beach was ice-covered and shore-fast ice was offshore, to early fall (Oct 6–8, 2014) when snow began to cover the landscape but offshore ice had yet to form and large storm waves still worked on the coast and bluffs (Fig. 4).

3.6. Meteorological data

Meteorological data (wind speed and direction, barometric pressure, air temperature) measured at Barter Island (NOAA, 2017b) and meteorological and water level and temperature data measured at Prudhoe Bay, the only continuously recording tide gauge in the area and located about 185 km west of Barter Island (NOAA, 2017c), illustrate environmental conditions at Barter Island beginning just prior to the initial SfM survey on July 1, 2014 and continuing to October 9, 2014. Wind, pressure, and water level data from Prudhoe Bay and Barter Island are intermittent after October 2014 and only temperature data are shown for the entire year. No water level or water temperature data, and only intermittent air temperature data after May 72,015 were available for Barter Island, however, the close correlation between pressure and winds suggest water levels as well as temperature at Barter Island would likely be similar to data recorded at Prudhoe Bay. Note that elevated water levels generally correspond to periods where winds are from west and wind speeds are high. Due to the Coriolis force, winds blowing from the west elevate water levels and winds from the east depress the water levels along the north coast of Alaska.

4. Results and discussion

4.1. Bluff change

Between July 1, 2014 and July 5, 2015, 38,100 ± 300 m^3 of material was eroded from the 3.2 km long section of permafrost bluffs on the Beaufort Sea Coast of Barter Island. The majority of material (70%) was lost during the summer of 2014 (July 1 to Sept 7) and the remaining 30% between the late summer and following winter-spring of 2014–15 (Sept 7, 2014 to July 5, 2015) (Table 3, Fig. 5). Most of the loss occurred along a 1.5 km stretch of coast within the central part of the study area (*"Central bluffs"* in Fig. 5). Significant but lower amounts of bluff erosion were measured on the western bluffs (*"Western bluffs"* in Fig. 5), and little overall change and accretion was measured along the bluffs on the eastern portion of the study area (*"Eastern bluffs"* in Fig. 5).

Retreat of the top of the bluff ranged from 0 to 8.1 m (mean 1.3 m) over the study period with the highest values measured in the central part of the bluffs during the summer of 2014 (Table 4; Fig. 6A). The base of the bluff retreated up to 7 m (mean 1.7 m), with nearly all transects eroding with the exception of the distal eastern bluffs where relatively extensive beaches front the bluffs and almost no change was observed (Figs. 6B, C) and the western end where accretion was measured where debris fans were deposited (Fig. 6B). Erosion of material at the base of the bluffs primarily occurred between July and September 2014 while accretion associated with the deposition of debris fans and talus deposits dominated between September 2014 and July 2015 (Fig. 6B).

Perspective views and profiles across the Barter Island bluffs illustrate this seasonal change in bluff morphology (Figs. 7 and 8). In July 2014, morphology varied from bluffs with a relatively gently sloping, convex profile from top to bottom (Figs. 7A and 8C, profile a-a') to relatively steep bluffs that were near-vertical and/or had an over-hanging peat visors at the top (Figs. 7A and 8C, profile b–b′). In both cases, a well-developed debris apron was present at the base of the bluffs. By September 2014, much of the material at the top of the bluffs had failed, the base of the bluff had steepened as the debris aprons were removed, and in places a niche had formed at the base of the bluff (Figs. 7B and 8A). By July 2015, the bluffs again had a profile similar to the previous

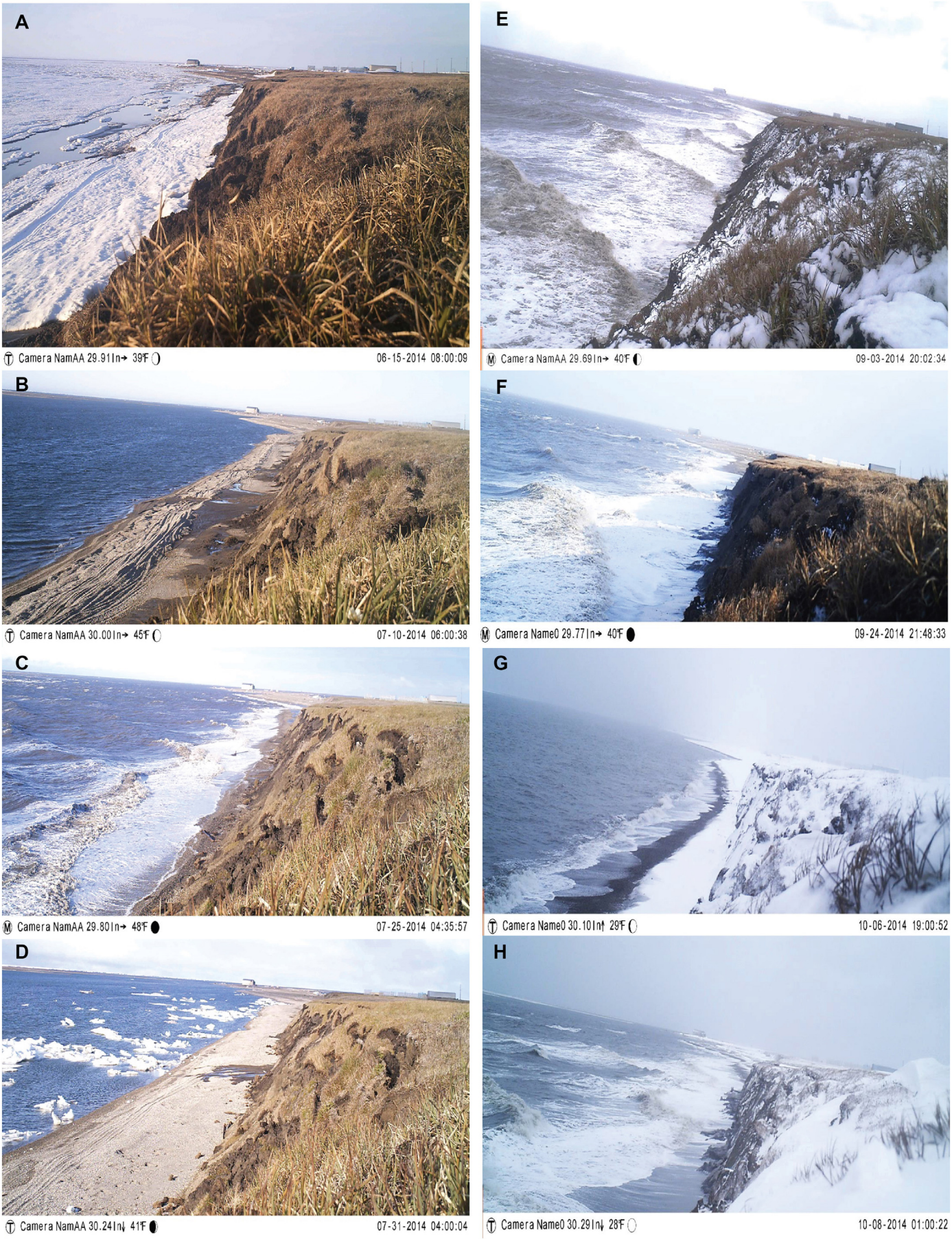
A
Camera NamAA 29.91In→ 39℉
06-15-2014 08:00:09
B
Camera NamAA 30.00In→ 45℉
07-10-2014 06:00:38
C
Camera NamAA 29.80In→ 48℉
07-25-2014 04:35:57
D
Camera NamAA 30.24In↓ 41℉
07-31-2014 04:00:04
E
Camera NamAA 29.69In→ 40℉
09-03-2014 20:02:34
F
Camera Name0 29.77In→ 40℉
09-24-2014 21:48:33
G
Camera Name0 30.10In↑ 29℉
10-06-2014 19:00:52
H
Camera Name0 30.29In↓ 28℉
10-08-2014 01:00:22

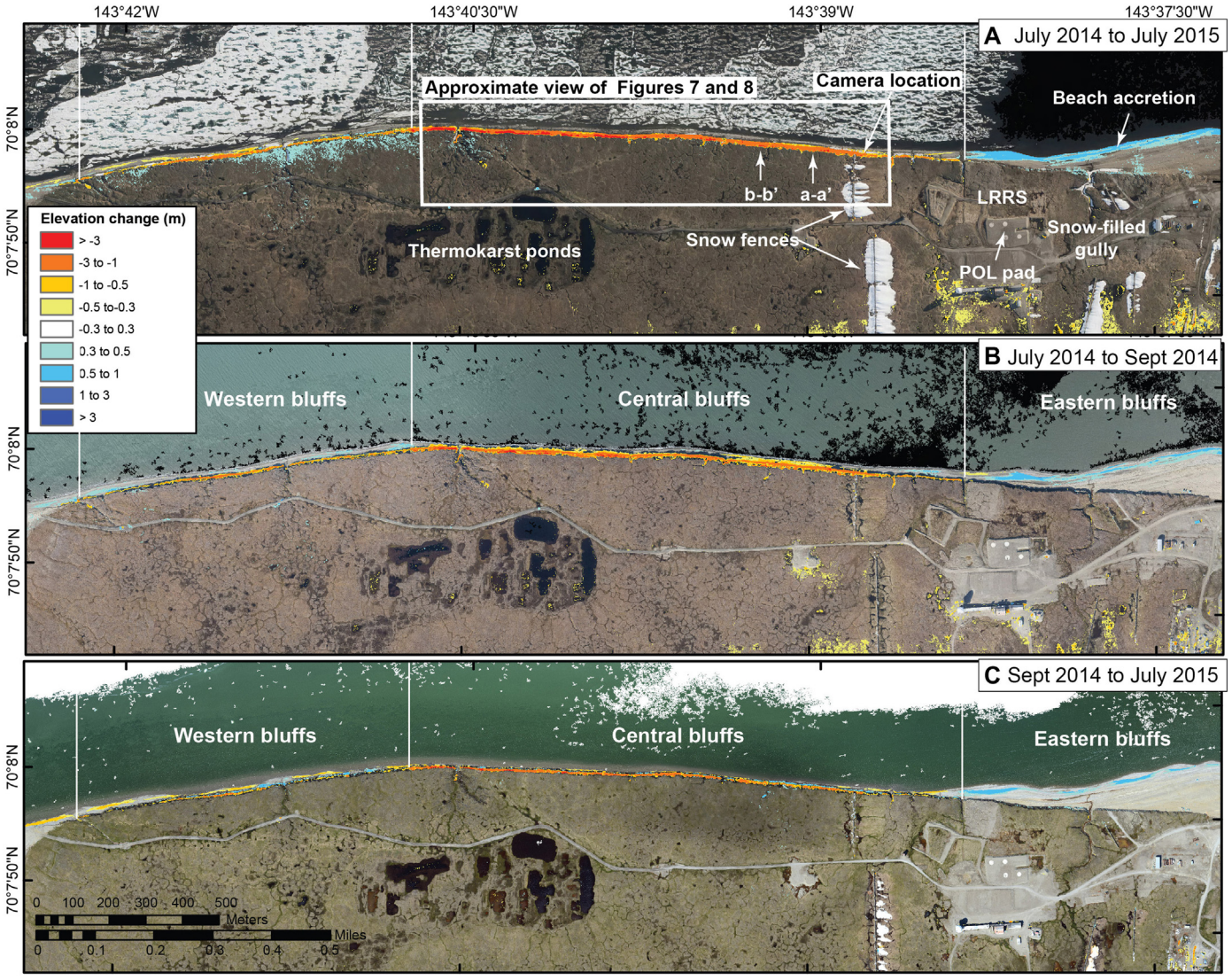

Fig. 5. Orthophotomosaics of the Barter Island bluff study area collected in A) July 2014, B) September 2014, and C) July 2015. Note in the July 2014 image the presence of ice offshore and ice and snow around snow fences, in gullies, and on the beach surface. The images are overlain with surface elevation difference values measured between July 2014 and 2015.

July, with a convex shape or relatively steep bluff face and top, and a debris apron at the base (Figs. 7C, 8B and C). The beach fronting the bluffs in July 2015 was strikingly narrow compared to the previous imagery.

4.2. Patterns and drivers of change: temperature, water level, and waves

The annual pattern of change to the Barter Island bluffs can be summarized as a combination of landward retreat of the bluff top and bluff face, likely through a combination of block failure, thaw slumping, sloughing and debris flows that accumulate at the base of the bluffs as distinct blocks or aggregated debris apron, and intermittent removal of the debris at the base of the bluffs by wave action. While these observed morphologic changes can fundamentally be reduced to thermal, mechanical, and thermo-mechanical processes, understanding the relative importance and interplay between them is challenging and difficult to quantify. We use meteorological and water level data, time-lapse camera imagery, and field observations from the summer of 2014 to provide insight into the probable timing of events and relative balance between processes responsible for the change observed.

4.2.1. Air and water temperature

Barter Island experienced 24 h of sunlight between May 17 and July 28, after which air temperature declined as daylight, solar heating, and insolation also declined (Fig. 9). Between the first 2 surveys, air temperature averaged 4.4 °C, reaching a maximum of 16.1 °C on July 21. The average air temperature was over 2 °C higher prior to July 28 (July 1 to July 28; 5.3 °C; range 0.6°–16.1 °C) compared to after July 28 (July 29 to Sept 7; average and 3.1 °C; range 0.6°–11.1 °C). Temperatures continued to

Fig. 4. Photographs from a mounted time-lapse camera looking eastward along Barter Island's north shore document coastal bluff, beach, and wave conditions during a single summer. View looking east; all photos from 2014. A. June 14, the beach is covered in ice and shorefast ice is present offshore; B. July 10, the beach and nearshore waters are ice-free. Ice push ridges are present on the forebeach and talus deposits and mudflows are forming on the upper beach. Note the camera has tilted due to movement of the material at the top of the bluffs; C. July 25, westerly waves erode the beach removing debris deposits but do not reach the base of the bluff. Note the slumping of the material of the top of the bluff; D. July31, easterly winds depress water levels forming a wide beach and bring ice-bergs close to shore; E. Sept 3, large westerly waves directly impact the base of the bluffs. Note the camera has tilted again due to movement of the bluffs. F. Sept 24, debris deposits at the base of the actively eroding bluffs; G. Oct 6, Snow covers the bluffs and beach, but sea-ice has not formed offshore allowing for large fall storm waves to continue to reach and erode the coastal bluffs (H, Oct 8).

Table 4
Net feature movement distance, in meters.

	All transects ($n = 317$)				Western bluff ($n = 97$)				Central bluff ($n = 153$)				Eastern bluff ($n = 67$)			
	Mean	Min	Max	StDev	Mean	Min	Max	StDev	Mean	Min	Max	StDev	Mean	Min	Max	StDev
Top of bluff																
Jul14 to Sep14	−0.8	1.4	−6.1	1.1	−0.5	1.4	−3.9	0.7	−1.3	0.5	−6.1	1.3	−0.2	0.2	−0.9	0.2
Sep14 to Jul15	−0.5	0.0	−3.4	0.6	−0.5	0.0	−2.5	0.4	−0.7	0.0	−3.4	0.6	−0.2	0.0	−0.3	0.1
Jul14 to Jul15	−1.3	0.3	−8.1	1.4	−1.0	0.3	−4.9	0.8	−2.0	0.3	−8.1	1.6	−0.2	0.0	−0.9	0.2
Base of bluff																
Jul14 to Sep14	−2.2	1.8	−6.1	1.7	−1.5	1.8	−5.6	1.6	−3.4	−0.5	−6.1	1.2	−0.4	0.1	−1.6	0.5
Sep14 to Jul15	0.5	6.0	−3.3	1.0	0.7	6.0	−3.3	1.4	0.5	2.7	−1.8	0.8	0.1	1.4	0.0	0.3
Jul14 to Jul15	−1.7	3.4	−7.0	1.7	−0.8	3.4	−5.6	1.5	−2.9	0.0	−7.0	1.3	−0.3	0.1	−1.6	0.5
Shoreline																
Jul14 to Sep14	0.0	20.8	−8.8	5.3	0.6	5.7	−3.8	2.3	−2.7	6.4	−8.8	3.2	5.4	20.8	−6.5	7.6
Sep14 to Jul15	−1.7	16.8	−12.5	6.0	−4.4	4.1	−11.4	2.8	−4.2	3.6	−12.5	3.3	7.8	16.8	1.3	4.6
Jul14 to Jul15	−1.7	30.9	−12.8	8.7	−3.8	1.8	−7.7	2.2	−6.8	−0.5	−12.8	2.0	13.2	30.9	0.7	7.3

[Min, minimum; Max, maximum; StDev, standard deviation; negative indicates erosion; positive indicates accretion].

drop after the September 7 survey throughout the fall and winter and were near or below 0 °C after October 9, which likely closely corresponds with the onset of sea-ice formation, as suggested by the stabilization of water temperatures at Prudhoe Bay around the same time. Throughout the winter air temperatures reach as low as −40 °C in early March when they begin to increase. Spring thawing, the onset of sea-ice breakup, and warming of air temperature beginning around May 20 can be inferred from the Prudhoe Bay record since only intermittent temperature information was recorded at Barter Island after May 7, 2015. Extremely high air temperatures of up 22 °C measured throughout the month of June 2015 at Prudhoe Bay suggest that temperatures at Barter Island were also high, and likely higher than the summer of 2014, which may reflect the lack of ice or snow cover in July 2015 imagery compared to July 2014 (Fig. 5).

4.2.2. Water level and wave impact

Time lapse images recorded between June 14 through Oct. 8, 2014 document a seasonal transition from an early summer ice-and-snow covered beach and nearshore, followed by alternating periods of quiescence and storminess, where wide beaches form and erode, bluffs slump and dewater as temperatures warm, debris aprons form at the base of the bluffs then erode as waves reach them, and finally snow covers the beach and bluffs in the fall (Fig. 4).

Elevated water levels along the Barter Island coast commonly results in flooding and overwash of low-lying areas and removal of sediment at the base of the permafrost bluffs triggering large-scale bluff failures. As an indicator of the frequency and duration of this type of thermo-mechanical erosion, time periods when waves were observed in the time lapse imagery (wave events) and when ocean water and/or

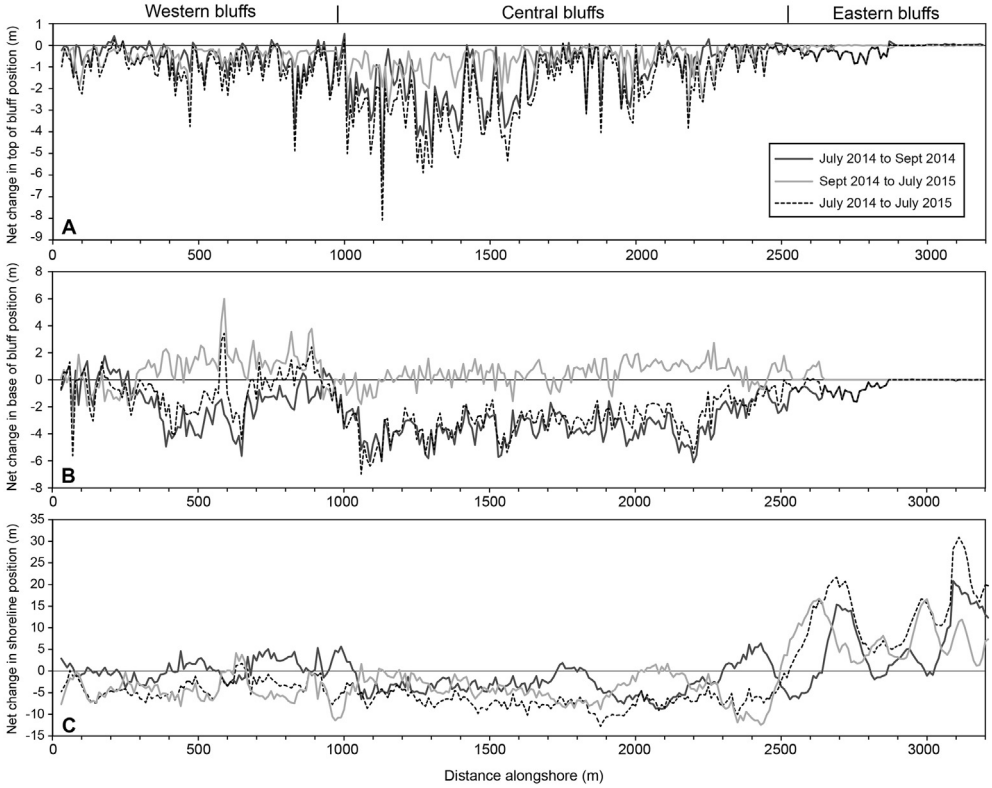

Fig. 6. Plots showing the net change in position of the top of bluff, base of bluff and the shoreline over the 3 time periods.

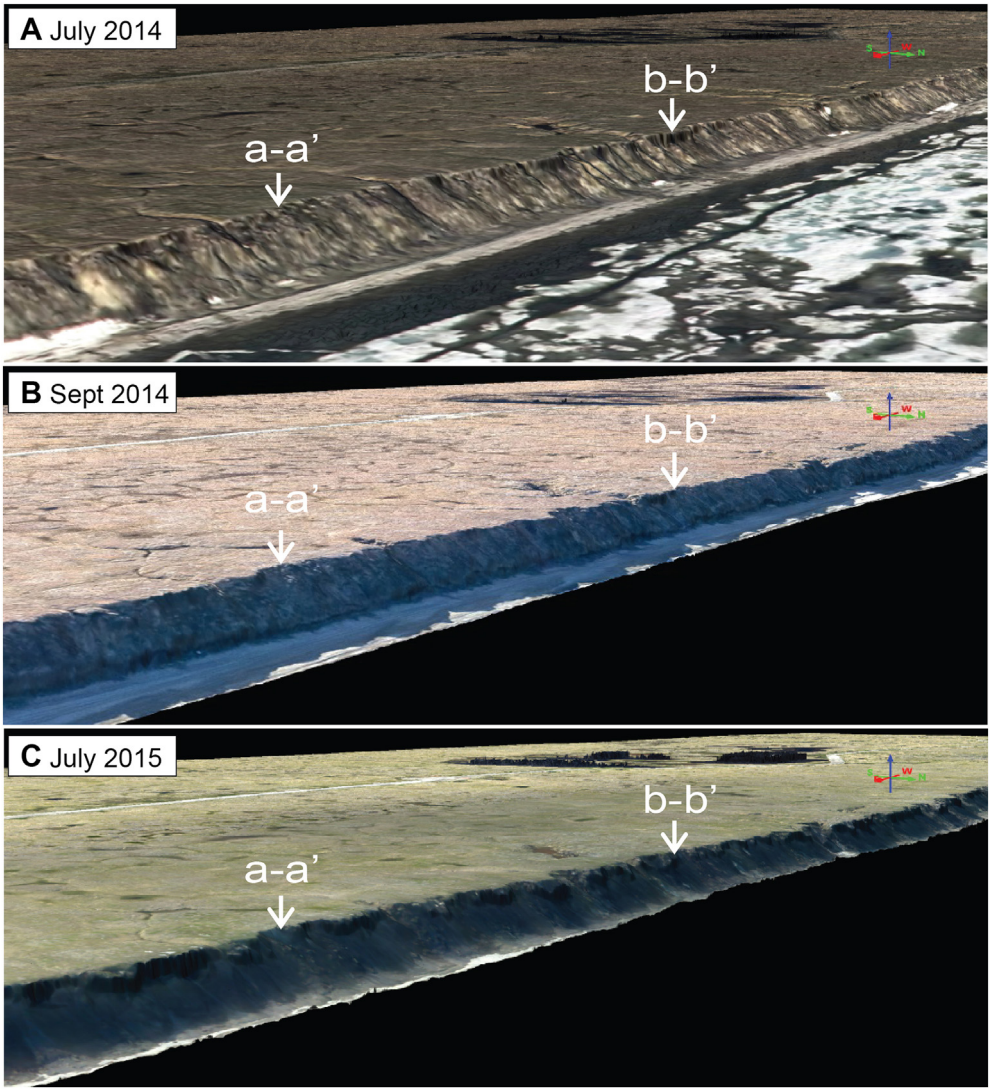

Fig. 7. Perspective views of the Barter Island bluffs showing the variation in bluff morphology during the study. Images are orthophotomosaics draped over elevation hillshade models and the view is to the southwest. Locations of the bluff profiles shown in Fig. 8 are indicated by the white arrows. Note the transition in morphology from early summer (July; A and C), where a well-developed debris apron at the base of the bluff is fronted by a narrow beach, compared to late summer (Sept; B), where a thermoerosional niche is present at the base of the bluffs and a relatively wide beach fronts the coast.

waves reached the base of the bluffs (bluff-impact events) were quantified and are plotted in Fig. 9 with the meteorological and water level data.

Between the first 2 surveys, 9 individual wave events were observed, ranging from approximately 8 to 98 h in duration (274 total hours). During those wave events, water and/or waves reached the base of the bluffs 4 times for a total of 106 h. Between September 8 and October 8, 2014, when image acquisition ended, some of the largest waves of the season were observed, with 5 wave events with durations between 19 and 84 h (213 total hours) 70 of those in which water and/or waves reached the base of the bluffs.

The field of view of the time-lapse camera is of the eastern end of the coastal bluffs where a moderately wide fronting beach was present throughout most of 2014 in contrast to central bluff section where erosion rates were higher and fronting beaches were typically narrow to non-existent throughout the year. Although exposed to the same wave events, it is likely that the central, and to a lesser extent the western bluffs, were impacted by waves more frequently than was observed in the time-lapse imagery.

Overall, both wave and bluff-impact events became more frequent and of longer duration as the summer progressed, with the longest period of sustained waves and bluff impact (77 h) occurring just prior to the September 07 survey. Hourly averaged water levels measured at Prudhoe Bay during this storm were elevated nearly 90 cm above mean-sea level, which is over 4 times the diurnal tidal range of 18 cm at Barter Island (NOAA, 2017a, NOAA, 2017c). No water levels were measured at Barter Island, however, wind speeds measured at Barter Island were on average 10 m/s stronger than at Prudhoe Bay (Fig. 9E). During this event, waves were also observed by the authors to be actively eroding the base of the bluffs. As water levels fell, near vertical walls and thermo-mechanical niches that had formed at the base of ice-rich bluffs became apparent, as can also be seen the September 07 imagery (Fig. 7B). Most of the pre-existing debris at the base of bluffs was removed during the storm but initiation of bluff-face debris flows and deposition of new debris at the base of the bluff and the back beach began soon after the storm.

Quantifying the relative contribution to the overall change from this event compared to previous or later events is not possible from the data sets described in this study since detailed morphological data are not available immediately preceding and following the other storm events. Because of the extended duration of elevated water levels, high waves, and associated bluff impact just prior to data collection, however, the

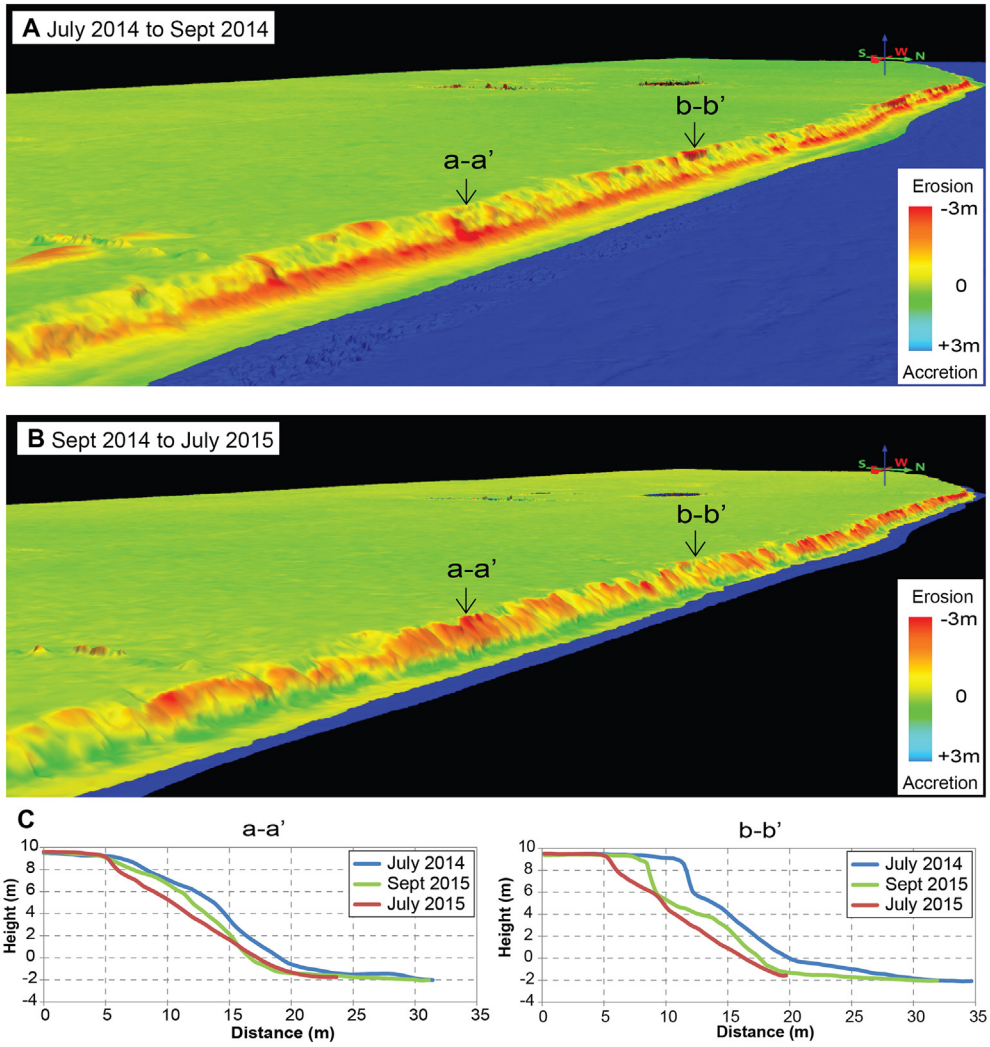

Fig. 8. Examples of elevation change patterns observed at Barter Island between July 2014 and 2015. Elevation difference plots from the 2 analysis periods showing A: a pattern dominated by retreat at the top of the bluffs and removal of the debris apron at the base between July 2014 and Sept 2014; and B: erosion over the entire bluff profile and deposition of material at the base between Sept 2014 and July 2015. Cross-shore profiles (C) suggest the bluffs maintain their overall shape as they retreat.

September survey may represent an end-member condition of the beach characterized by a nearly debris-apron-free beach and deep thermo-erosional niches at the base of the bluffs.

4.3. Sediment budget and annual signals

The volume of material lost from the bluffs between July and September does not provide a complete estimate of total volume change over the ice-free season. At least 6 wave events and 3 bluff-impact events occurred after the September 7 survey and prior to the onset of ice formation in early October (Fig. 9). It is likely that most of the volume loss measured between the September 2014 and July 2015 surveys occurred during this time as waves continued to reach the base of the bluffs and remove material. Although warm air temperatures observed at Prudhoe in June 2015 likely contributed to thermal erosion and overall morphological change to the bluffs (Fig. 8B), any material eroded from the bluffs after the formation of ice in the fall of 2014 was likely deposited in the debris apron at the base of the bluffs and is included in the net volume change calculations. Thus, we suggest that the net annual volume change of 38,100 ± 300 m^3, or 1.3 m^3/m, is a representative estimate for both annual and ice-free season components of the Barter Island, permafrost bluffs sediment budget. An additional potential contribution to the sediment budget is the addition or removal of material from the beach and bluffs through long-shore sediment transport and the entrainment and transport by surface ice (Reimnitz et al., 1987; Kempema et al., 1989; Osterkamp and Gosink, 1984; Eicken et al., 2005). Quantifying this process was beyond the scope of this study, however, it could be significant and remains an unknown contributor to the annual sediment budget.

The ability to compare results presented here with previous years and/or long-term trends is difficult because previous assessments of coastal change on Barter Island focused on 2-dimensional (horizontal) change in the position of the shoreline or bluff edge rather than a 3-dimensional change in the position and morphology of the bluffs as in this study. Long-term shoreline change rates of the coast fronting the Barter Island permafrost bluffs averaged −1.2 ± 0.2 m/yr (range − 1.8 to +0.2 m/yr) between 1947 and 2012 (Gibbs and Richmond, 2017), which is a somewhat lower rate compared to the mean change in shoreline position of −1.7 m (range − 12.0 to +30.9 m, Table 4) measured during this study. The long-term rate of change of the top bluff edge averaged −1.5 ± 0.1 m/yr; (range − 2.2 to −0.4 m/yr) between 1955 and 2015 (Gibbs et al., 2018) which is similar, although slightly higher than the mean horizontal change in the position of the top of the bluff (−1.3 m; range: −8.1 to +0.0 m/yr, Table 4) measured in this study. Comparison of the long-term rates of change with the horizontal feature change measured in this study suggests that the 2014–

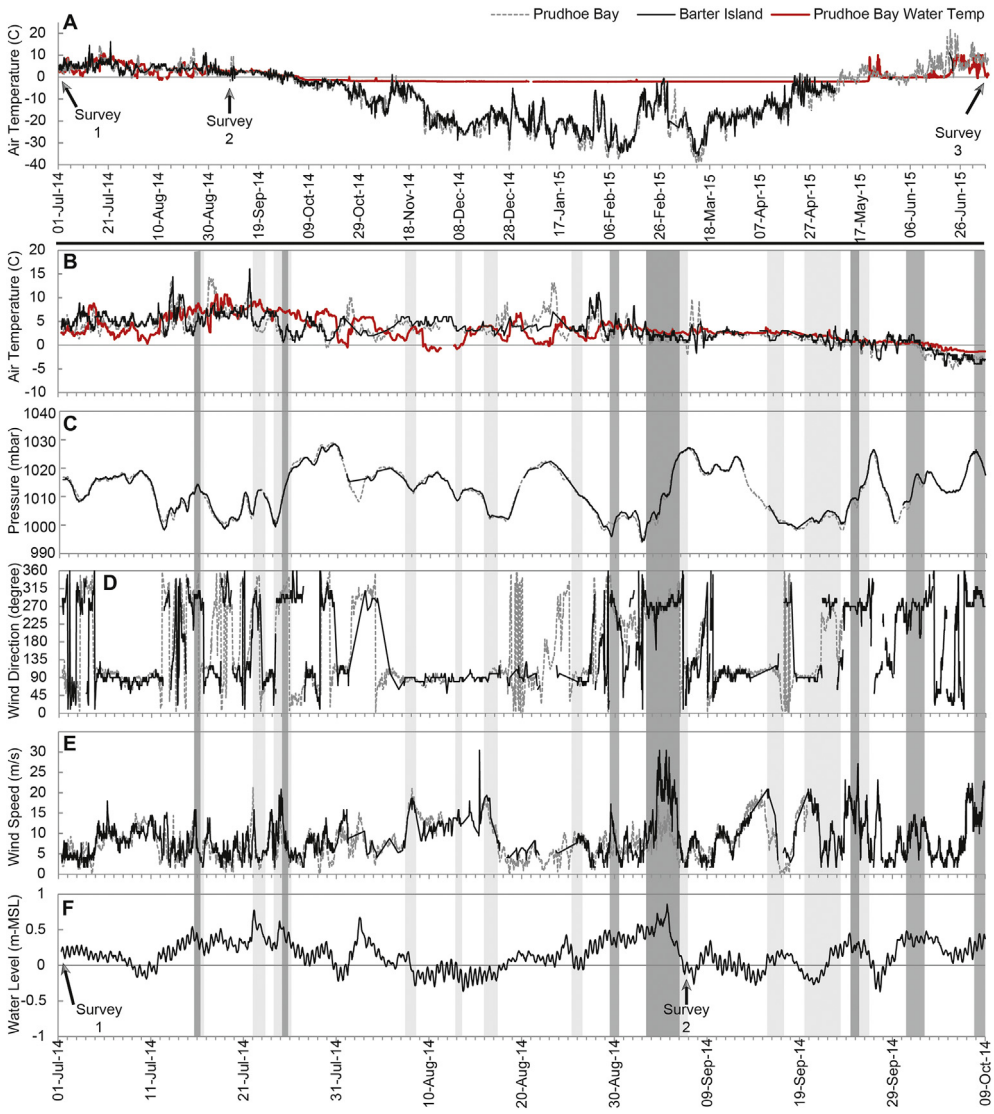

Fig. 9. Meteorological and water level data measured at Barter Island (NOAA, 2017b) and Prudhoe Bay tide gauge (NOAA, 2017c) during (A) the study period, July 12, 2014 to July 4, 2015 and (B–F) the mid-summer to early-fall of 2014. Arrows show dates of aerial image acquisition. Light gray vertical bars indicate time when waves were observed in the time lapse imagery and dark gray bars indicate time when water or waves were observed to reach the base of the bluffs.

2015 year represented relatively typical or slightly below average conditions.

4.4. Patterns and mechanisms of change

Drivers of the observed change to the permafrost bluffs are likely a combination of thermal and mechanical processes. Sustained thermal erosion to the bluff surface due to warming air temperature and solar radiation in early to mid-summer of 2014 caused debris flows and thaw slumping leading to deposition of a debris apron at the base and over steepening of the top of the bluffs. This was followed by a mid to late summer/early fall 2015 pattern of episodic thermo-mechanical removal of material, niching, and undercutting of the base associated with high-water levels and waves driven by low-pressure storms and easterly winds and secondarily retreat of the bluffs from thermally induced debris flows, thaw slumping and block failure. From fall 2014 through the following winter and spring 2015, only moderate erosion of the bluff face occurred, with little overall retreat of the top edge of the bluff, and deposition of a narrow debris apron deposited at the base of the bluffs. It should be noted that although this is likely a typical seasonal pattern, the thermal and mechanical-driven processes can occur at any time during the ice-free summer depending on the relative timing of storm events and seasonal temperature patterns.

Based on the morphologic changes observed and temperature and wave-impact records described above, we propose a pattern of seasonal change where thermal processes, primarily indicated by bluff dewatering, surface sloughing and thaw slumping, and formation of overhanging visors, likely occurs throughout the ice-free season, but with a relatively larger influence earlier in the season when air temperatures are warmer, daylight is longer, storms are less frequent, and waves rarely reach and erode material from the base of the bluffs (Fig. 9). As the ice-free season continues through the summer and into early fall, mechanical and thermo-erosional processes begin to dominate as daylight wanes, temperatures decrease, and numerous large and powerful storms bring waves that erode material from the base of the bluffs and undercut the base through thermo-erosional niching. The loss of the bluff toe and niche-development leads to destabilization of the overlying bluff material, which can lead to large block failures, rotational slumps, and surface sloughing. Debris aprons develop quickly once waves recede from the base of the bluffs, but likely little change occurs to the bluffs or debris aprons once sea-ice formation is initiated and is present to protect the coast.

The causes of the variation in bluff morphology are not well-constrained and require additional observation and research but are likely due to variations in bluff physical properties through a combination of ice content, sediment grain size, cohesion, and associated failure modes. The presence or absence of a beach is an important feature for modulating both seasonal and longer-term bluff change. When present, the beach provides protection to the bluffs from direct wave impact as long as beach elevation and width limit the total water level, including wave run-up, from reaching the base of the bluff. Over the course of the study, sand to gravel sized beach deposits fronting most of the Barter Island bluffs were observed to form and erode over a variety of timescales. Despite the large amount of sand and gravel eroding from the bluffs, only in the eastern section was an extensive beach persistent throughout the study period. In this area, the beach prograded over 30 m, and minimal bluff retreat was measured, highlighting the importance of beach width on bluff stability (Figs. 5 and 6). Beach development and stability and the fate of the eroding bluff sediment at Barter Island requires further study and is beyond the scope of this paper. However, the presence of the extended spits on both sides of the island and nearly bi-directional winds and currents measured at BTI (Barnes et al., 1987; Erikson et al., in press) suggest that processes driving change are likely a combination of along-shore transport and deposition of eroded bluff material associated with westerly winds and waves in competition with easterly transport by easterly waves and wave refraction around Bernard Spit. In all likelihood, the depositional process likely fluctuates both annually and over longer time periods in response to changes in sediment availability and larger oceanographic patterns.

The steep, vertical bluffs at Barter Island typically have higher ice content throughout, but in particular have 1–3 m thick, segregated ice layers near the top which melt, leaving resulting in the unsupported overhanging peat visor (Fig. 2). When the overhanging visors fail, the apparent landward retreat of the bluff top is rapid and ablation of the underlying bluff material increases due to exposure to wind, water, solar radiation, and warm air. The ice content and composition of the lower angle convex bluff profiles is more difficult to determine because the bluff face is typically obscured by a mélange of slumped debris material including sediment and vegetation mats. Large block failures associated with undercutting and destabilization of the base of the bluff, as well as formation of debris aprons at the base of the bluffs, do not seem to depend on precedent bluff profile.

5. Conclusions

- Structure-from-motion photogrammetry was used to create very high-resolution and precise orthophotomosaics and digital surface models for measuring fine-scale, annual changes in coastal bluff position, volume, and morphology at Barter Island, Alaska.
- The method provides high-quality, detailed data that is relatively low cost compared to traditional airborne lidar surveys, is more rapid and comprehensive compared to ground-based GPS surveys, and is readily scalable to large regional data collections, where use of unmanned aircraft systems (UAS) is impractical (for example, Overbeck et al., 2016).
- 38,100 $\pm$ 300 m^3 (1.3 m^3/m) of material was eroded from the Barter Island bluffs between July 2014 and 2015. The majority (70%) was lost during the early summer of 2014 (July 1 to Sept 7) with the remainder removed during the late summer and following winter-spring (Sept 7, 2014 to July 5, 2015).
- Comparison of the observed annual change with long-term (>60 year) average change suggests that the 2014–2015 year represented relatively typical or slightly below average conditions.
- Drivers of the observed change are likely a combination of thermal and mechanical processes with thermal erosional processes (debris flows, thaw slumping, and oversteepening of the top of the bluffs) likely dominating in early to mid-summer and episodic thermal mechanical removal of material, niching, and undercutting of the base of the bluff dominating in mid-late summer to early fall. Although this is likely a typical seasonal pattern, the thermal and mechanical-driven processes can occur at any time during the ice-free summer depending on the relative timing of storm events and seasonal temperature patterns.

Despite the limited duration of this study, the results illustrate how rapidly this high-latitude coast is changing, with bluff retreat rates that are many times greater than typical rates observed for lower latitude coastal systems. This study provides only a general framework for evaluating the important processes and drivers of morphological change to permafrost bluffs. Future efforts focused on quantifying the direct impact of solar radiation and temperature gradients on bluff erosion rates, in addition to observational data on wave impact and response, are required to better understand the relative balance and interplay between thermal and mechanical processes in permafrost bluff change, which are critical components of future modeling efforts and coastal change projections, particularly in a warming climate.

Funding source: This work was supported by the U.S. Geological Survey, Coastal/Marine Hazards and Resources Program, Coastal National Elevation Database Science Applications, Climate Change Impacts on High-latitude Coasts, and National Assessment of Coastal Change Hazards Projects.

Acknowledgements

This work was supported by the U.S. Geological Survey, Coastal and Marine Geology Program, Coastal National Elevation Database Science Applications, Climate Change Impacts on High-latitude Coasts, and National Assessment of Coastal Change Hazards Projects. The authors would like to thank P. Barnard and J. Warrick of the USGS and anonymous reviewers for thoughtful comments that improved this paper.

References

Aré, F.E., 1988. Thermal abrasion of sea coasts. Polar Geogr. Geol 12, 1–157. https://doi.org/10.1080/10889378809377343.

Barnes, P.W., Graves, S., Reimnitz, E., 1987. Beaufort Sea coastal currents: a divergence near Barter Island, Alaska? In: Hamilton, T.D., Galloway, J.P. (Eds.), Geologic studies in Alaska by the U.S. Geological Survey during 1986. 998. U.S. Geological Survey Circular, pp. 139–142. https://doi.org/10.3133/cir998

Barnhart, K.R., Overeem, I., Anderson, R.S., 2014. The effect of changing sea ice on the physical vulnerability of Arctic coasts. Cryosphere 8, 1777–1799. https://doi.org/10.5194/tc-8-1777-2014.

Eicken, H., Gradinger, R., Gaylord, A., Mahoney, A., Rigor, I., Melling, H., 2005. Sediment transport by sea ice in the Chukchi and Beaufort Seas: increasing importance due to changing ice conditions? Deep Sea Res. II 52, 3281–3302. https://doi.org/10.1016/j.dsr2.2005.10.006.

Erikson, L.H., Gibbs, A.E., Richmond, B.M., Storlazzi, C.D., Jones, B.M., Ohman, K.A., 2019. Changing storm conditions in response to projected 21st century climate change scenarios and the potential impact on an Arctic barrier island-lagoon system — A pilot study for Arey Island and Lagoon, eastern Arctic Alaska. U.S. Geological Survey Open File Report (in press).

ESRI, 2014. ArcGIS Desktop: Release 10.2.2. Environmental Systems Research Institute, Redlands, CA.

Fletcher, C.H., Romine, B.M., Genz, A.S., Barbee, M.M., Dyer, M., Anderson, T.R., Lim, S.C., Vitousek, S., Bochicchio, C., Richmond, B.M., 2012. National assessment of shoreline change: historical shoreline change in the Hawaiian Islands. U.S. Geological Survey Open-File Report 2011–1051, 55 https://doi.org/10.3133/ofr20111051.

Gibbs, A.E., Richmond, B.M., 2015. National assessment of shoreline change — Historical shoreline change along the north coast of Alaska, U.S. — Canadian border to Icy Cape. U.S. Geological Survey Open-File Report 2015–1048 https://doi.org/10.3133/ofr20151048.

Gibbs, A.E., Richmond, B.M., 2017. National assessment of shoreline change — Summary statistics for updated vector shorelines and associated shoreline change data for the north coast of Alaska, U.S. — Canadian border to Icy Cape. U.S. Geological Survey Open-File Report 2017–1107 https://doi.org/10.3133/ofr20171107.

Gibbs, A.E., Nolan, M., Richmond, B.M., 2016. Evaluating changes to arctic coastal bluffs using repeat aerial photography and structure-from-motion elevation models. Proceedings from 2015 Coastal Sediments Conference, San Diego CA, May 2015. CD-ROM. https://doi.org/10.1142/9789814689977_0080.

Gibbs, A.E., Richmond, B.M., Erikson, L.H., Jones, B.M., 2018. Long-term retreat of coastal permafrost bluffs, Barter Island, Alaska. In: Deline, P., Bodin, X., Ravanel, L. (Eds.), 5th European Conference on Permafrost. Chamonix, France, pp. 798–799.

Gibbs, A.E., Nolan, M., Snyder, A.G., 2019. Orthophotomosaics, elevation point clouds, digital surface elevation models, and supporting data from the north coast of Barter Island. Alaska. U.S. Geological Survey data release. https://doi.org/10.5066/P9964TKX.
Guégan, E.B.M., Christiansen, H.H., 2017. Seasonal Arctic coastal bluff dynamics in Adventfjorden, Svalbard. Permafr. Periglac. Process. 28, 18–31. https://doi.org/10.1002/ppp.1891.
Günther, F., Overduin, P.P., Sandakov, A.V., Gross, G., Grigoriev, M.N., 2013. Short- and long-term thermos-erosion of ice-rich permafrost coasts in the Laptev Sea region. Biogeosciences 10, 4297–4318. https://doi.org/10.5194/bg-10-4297-2013.
Hapke, C.J., Himmelstoss, E.A., Kratzmann, M.G., List, J.H., Thieler, E.R., 2011. National assessment of shoreline change; historical shoreline change along the New England and Mid-Atlantic coasts. U.S. Geological Survey Open-File Report 2010–1118 https://doi.org/10.3133/ofr20101118.
Himmelstoss, E.A., Kratzmann, M.G., Thieler, E.R., 2017. National assessment of shoreline change - Summary statistics for updated vector shorelines and associated shoreline change data for the Gulf of Mexico and Southeast Atlantic coasts. U.S. Geological Survey Open-File Report 2017–1015 https://doi.org/10.3133/ofr20171015.
Hopkins, D.M., Hartz, R.W., 1978. Coastal morphology, coastal erosion, and barrier islands of the Beaufort Sea, Alaska. U.S. Geological Survey Open-file Report 78–1063 https://doi.org/10.3133/ofr781063.
Hoque, M.A., Pollard, W.H., 2009. Arctic coastal retreat through block failure. Can. Geotech. J. 46, 1103–1115. https://doi.org/10.1139/T09-058.
Irrgang, A.M., Lantuit, H., Manson, G.K., Günther, F., Grosse, G., Overduin, P.P., 2018. Variability in rates of coastal change along the Yukon coast, 1951 to 2015. J. Geo. Res. Earth Surface. 123, 779–800. https://doi.org/10.1002/2017JF004326.
Isaev, V.S., Koshurnikov, A.V., Pogorelov, A., Amangurov, R.M., Podchasov, O., Sergeev, D.O., Buldovich, S.N., Aleksyutina, D.M., Grishakina, E.A., Kioka, A., 2018. Cliff retreat of permafrost coast in the southwest Baydaratskaya Bay of Kara Sea during 2005–2016. Permafrost Periglac. Process. 30, 35–47. https://doi.org/10.1002/ppp.1993.
Jones, B.M., Farquharson, L.M., Baughman, C.A., et al., 2018. A decade of remotely sensed observations highlight complex processes linked to coastal permafrost bluff erosion in the Arctic. Env. Res. Lett. 13. https://doi.org/10.1088/1748-9326/aae471.
Jorgenson, M.T., Brown, J., 2005. Classification of the Alaskan Beaufort Sea Coast and estimation of carbon and sediment inputs from coastal erosion. Geo-Mar. Lett. 25, 69–80. https://doi.org/10.1007/s00367-004-0188-8.
Kanevskiy, M., Shur, Y., Jorgenson, M.T., Ping, C.L., Michaelson, G.J., Fortier, D., Stephani, E., Dillon, M., Tumskoy, V., 2013. Ground ice in the upper permafrost of the Beaufort Sea coast of Alaska. Cold Reg. Sci. Technol. 85, 56–70 ISSN 0165-232X. https://doi.org/10.1016/j.coldregions.2012.08.002.
Kempema, E.W., Reimnitz, E., Barnes, P.W., 1989. Sea ice entrainment and rafting in the Arctic. J. Sediment. Petrol. 59, 308–317. https://doi.org/10.1306/212F8F80-2B24-11D7-8648000102C1865D.
Koenderink, J.J., van Doorn, A.J., 1991. Affine structure from motion. J. Opt. Soc. Am. 82, 377–385.
Lantuit, H., Overduin, P.P., Couture, N., Wetterich, S., Aré, F., Atkinson, D., Brown, J., Cherkashov, G., Drozdov, D., Forbes, D.L., 2012. The Arctic coastal dynamics database: a new classification scheme and statistics on Arctic permafrost coastlines. Estuar. Coasts 35, 383–400. https://doi.org/10.1007/s12237-010-9362-6.
Lantuit, H., Overduin, P.P., Wetterich, S., 2013. Recent progress regarding permafrost coasts. Permafrost Periglac. Process. 24, 120–130. https://doi.org/10.1002/ppp.1777.
Leffingwell, E. de K., 1919. The Canning River region of northern Alaska U.S. Geol. Surv. Prof. Pap. 109. https://doi.org/10.3133/pp109.
Liu, L., Larson, K.M., 2018. Decadal changes of surface elevation over permafrost area estimated using reflected GPS signals. Cyrosphere 12, 477–489. https://doi.org/10.5194/tc-12-477-2018.
Morton, R.A., Miller, T.L., Moore, L.J., 2004. National assessment of shoreline change: Part 1, historical shoreline changes and associated coastal land loss along the U.S. Gulf of Mexico. U.S. Geological Survey Open-File Report 2004–1043 https://doi.org/10.3133/ofr20041043.
National Oceanic and Atmospheric Administration, 2017a. Tides and Currents— Barter Island, AK—Station ID 9499176, National Oceanic and Atmospheric Administration Web Site. accessed February 18, 2017. https://tidesandcurrents.noaa.gov/stationhome.html?id=9499176.
National Oceanic and Atmospheric Administration, 2017b. NOAA National Centers for Environmental Information Web Site. accessed February 18, 2017. https://www.ncdc.noaa.gov/data-access/land-based-station-data/land-based-datasets/quality-controlled-local-climatological-data-qclcd.
National Oceanic and Atmospheric Administration, 2017c. Tides and Currents— Prudhoe Bay, AK—Station ID 9497645, National Oceanic and Atmospheric Administration Web Site. accessed February 18, 2017. http://tidesandcurrents.noaa.gov/stationhome.html?id=9497645.
Nolan, M., DesLauriers, K., 2016. Which are the highest peaks in the US Arctic? Fodar settles the debate. Cryosphere 10, 1245–1257. https://doi.org/10.5194/tc-10-1245-2016.
Nolan, M., Larsen, C.F., Sturm, M., 2015. Mapping snow-depth from manned-aircraft on landscape scales at centimeter resolution using Structure-from-Motion photogrammetry. Cryosphere 9, 1445–1463. https://doi.org/10.5194/tc-9-1445-2015.
Novikova, A., Belova, N., Baranskaya, A., Aleksyutina, D., Maslakov, A., Zelenin, E., Shabanova, N., Ogorodov, S., 2018. Dynamics of permafrost coasts of Baydaratskaya Bay (Kara Sea) based on multi-temporal remote sensing data. Remote Sens. 10, 1481.
Obu, J., Lantuit, H., Grosse, G., Günther, F., Sachs, T., Helm, V., Fritz, M., 2017. Coastal erosion and mass wasting along the Canadian Beaufort Sea based on annual airborne LiDAR elevation data. Geom. 293, 331–346. https://doi.org/10.1016/j.geomorph.2016.02.014.
Osterkamp, T.E., Gosink, J.P., 1984. Observations and analysis of sediment laden sea ice. In: Barnes, P.W., Scholl, D.M., Reimnitz, E. (Eds.), The Alaska Beaufort Sea: Ecosystems and Environments. Academic Press, Orlando, FL, pp. 73–94.
Overbeck, J.R., Hendricks, M.D., Kinsman, N.E.M., 2016. Photogrammetric digital surface models and orthoimagery for 26 coastal communities of western Alaska. Alaska Division of Geological and Geophysical Surveys Raw Data File 2016-1 https://doi.org/10.14509/29548.
Overduin, P.P., Strzelecki, M.D., Grigoriev, M.N., Couture, N., Lantuit, H., St-Hilaire-Gravel, D., Günther, F., Wetterich, S., 2014. Coastal changes in the Arctic. In: Martini, I.P., Wanless, H.R. (Eds.), Sedimentary Coastal Zones from High to Low Latitudes: Similarities and Differences. 388, pp. 103–129. https://doi.org/10.1144/SP388 Geological Society, London, Special Publications.
Overeem, I., Anderson, R.S., Wobus, C.W., Clow, G.D., Urban, F.E., Matell, N., 2011. Sea ice loss enhances wave action at the Arctic coast. Geophys. Res. Lett. 38, L17503. https://doi.org/10.1029/2011GL048681.
Penland, S., Roberts, H.H., Williams, S.J., Sallenger, A.H., Cahoon, D.R., Davis, D.W., Groat, C.G., 1990. Coastal land loss in Louisiana. Trans. Gulf Coast Assoc. Geol. Soc. 40, 685–699.
Rawlinson, S.E., 1993. Surficial geology and morphology of the Alaskan Central Arctic Coastal Plain: Alaska Division Geological and Geophysical Survey, Fairbanks, AK, Report of Investigations, 93–11.
Reimnitz, E., Maurer, D.K., 1979. Effects of storm surges on the Beaufort Sea coast, northern Alaska. Arctic 324, 329–344.
Reimnitz, E., Kempema, E.W., Barnes, P.W., 1987. Anchor ice, seabed freezing, and sediment dynamics in shallow arctic seas. J. Geo. Res. 92 (C13), 14671–14678. https://doi.org/10.1029/JC092iC13p14671.
Reimnitz, E., Graves, S.M., Barnes, P.W., 1988. Beaufort Sea coastal erosion, sediment flux, shoreline evolution, and the erosional shelf profile. U.S. Geological Survey Miscellaneous Investigations Series, 22 https://doi.org/10.3133/i1182G Report I-1182-G.
Shiklomanov, N.I., Streletskiy, D.A., Little, J.D., Nelson, F.E., 2013. Isotropic thaw subsidence in undisturbed permafrost landscapes. Geophys. Res. Lett. 40, 6356–6361. https://doi.org/10.1002/2013GL058295.
State of Alaska, 2015. Department of Commerce, Community, and Economic Development, Community and Region Affairs Web Site. http://commerce.state.ak.us/dcra/DCRAExternal/community, Accessed date: 18 February 2017.
Sultan, N.J., Braun, K.W., Thieman, D.S., 2011. North Slope trends in sea level, storm frequency, duration and intensity. Ice Tech Conference, Prudhoe Bay, Paper No. ICETECH10-155-R0.
Thieler, E.R., Himmelstoss, E.A., Zichichi, J.L., Ergul, A., 2009. Digital Shoreline Analysis System (DSAS) version 4.0 - An ArcGIS extension for calculating shoreline change. U.S. Geological Survey Open-File Report 2008–1278 https://doi.org/10.3133/ofr20081278.
U.S. Geological Survey, 2015. AK_NORTHSLOPE Lidar Data Set, Available at USGS EarthExplorer Web Site. accessed February 18, 2017. http://earthexplorer.usgs.gov.
Western Regional Climate Center, 2008. Web site accessed February 18, 2017. https://wrcc.dri.edu/.
Westoby, M.J., Brasington, J., Glasser, N.F., Hambrey, M.J., Reynolds, J.M., 2012. 'Structure-from-Motion' photogrammetry: a low-cost, effective tool for geoscience applications. Geomorphology 179, 300–314. https://doi.org/10.1016/j.geomorph.2012.08.021.
Wiseman, W.J. Jr., Coleman, J.M., Gregory, A., Hsu, S.A., Short, A.D., Suhayda, J.N., Walters, C.D. Jr., Wright, L.D., 1973. Alaskan Arctic coastal processes and morphology. Louisiana State University, Coastal Studies Institute Technical Report No. 140.
Wobus, C., Anderson, R., Overeem, I., Natell, N., Clow, G., Urban, F., 2011. Thermal erosion of a permafrost coastline: improving process-based models using time-lapse photography. Arct. Antarct. Alp. Res. 43 (3), 474–484. https://doi.org/10.1657/1938-4246-43.3.474.
Zhang, J., Liu, F., Tao, W., Krieger, J., Shulski, M., Zhang, X., 2016. Mesoscale climatology and variation of surface winds over the Chukchi–Beaufort coastal areas. J. Clim. 29, 2721–2739. https://doi.org/10.1175/JCLI-D-15-0436.1.